



ELSEVIER

Available online at www.sciencedirect.com

SciVerse ScienceDirect

Proceedings of the Combustion Institute 34 (2013) 2683–2690

Proceedings
of the
Combustion
Institute

www.elsevier.com/locate/proci

Unwanted combustion enhancement by $C_6F_{12}O$ fire suppressant [☆]

Gregory T. Linteris ^{a,*}, Valeri I. Babushok ^a, Peter B. Sunderland ^b,
Fumi Takahashi ^c, Viswanath R. Katta ^d, Oliver Meier ^e

^a Fire Research Division, National Institute of Standards and Technology, Gaithersburg, MD 20899-8665, USA

^b Dept. of Fire Protection Engineering, The University of Maryland, College Park, MD 20742, USA

^c Case Western Reserve University, Cleveland, OH 44106, USA

^d Innovative Scientific Solutions, Inc., Dayton, OH 45440, USA

^e The Boeing Company, Seattle, WA 98124, USA

Available online 17 August 2012

Abstract

Several agents are under consideration to replace CF_3Br for use in suppressing fires in aircraft cargo bays. In a Federal Aviation Administration (FAA) performance test simulating the explosion of an aerosol can, however, the replacements, when added at sub-inerting concentrations, have all been found to create higher pressure rise than with no agent, hence failing the test. Thermodynamic equilibrium calculations as well as perfectly-stirred reactor (PSR) simulations with detailed reaction kinetics, are performed for one of these agents, $C_6F_{12}O$ (Novec 1230), to understand the reasons for the unexpected enhanced combustion rather than suppression. The high pressure rise with added agent is shown to depend on the amount of agent, and can only occur if a large fraction of the available oxidizer in the chamber is consumed, corresponding to stoichiometric proportions of fuel, oxygen, and agent. A kinetic model for the reaction of $C_6F_{12}O$ in hydrocarbon–air flames has been developed. Stirred-reactor simulations predict that at higher agent loadings, the inhibition effectiveness of $C_6F_{12}O$ is relatively insensitive to the overall stoichiometry, and the marginal inhibitory effect of the agent is greatly reduced, so that the mixture remains flammable over a wide range of conditions corresponding to those of the FAA test. The present findings are consistent with and support the earlier analyses for C_2HF_5 and CF_3Br , which were also evaluated in the FAA test. Published by Elsevier Inc. on behalf of The Combustion Institute.

Keywords: $C_6F_{12}O$; Novec 1230; Cargo bay fire suppression; Halon replacements; CF_3Br

[☆] Official contribution of NIST, not subject to copyright in the United States. Certain commercial equipment, instruments, and materials are identified in this paper to adequately specify the procedure. Such identification does not imply recommendation or endorsement by the National Institute of Standards and Technology.

* Corresponding author. Address: National Institute of Standards and Technology, Engineering Laboratory, 100 Bureau Dr., Stop 8665, Gaithersburg, MD 20899-8665, USA. Fax: +1 301 975 4052.

E-mail address: linteris@nist.gov (G.T. Linteris).

1. Introduction and background

Production of the fire suppressant CF_3Br (Halon 1301) has been banned by the Montreal Protocol because of its destruction of stratospheric ozone. Although a critical-use exemption has been granted to the aviation industry for use of recycled halon in cargo bay fire suppression, the European Union requires replacement of halon in new-design aircraft by 2018, and in

existing aircraft by 2040. Several replacements have been proposed, but they have all been found to enhance burning in the US Federal Aviation Administration (FAA) aerosol can test (FAA-ACT) [1], and hence they fail FAA's Minimum Performance Standard [2]. In particular, C_2HF_5 , $C_3H_2F_3Br$ (2-BTP), and $C_6F_{12}O$ [3] all produce higher peak pressures in a simulated cargo bay, as compared to no added agent, when they are added at concentrations less than that required to completely suppress the explosion. In contrast, addition of CF_3Br at sub-suppressing concentrations does not increase the pressure rise.

Enhanced combustion in the presence of fire suppressants has been noted in previous studies. A promotion or inhibition effect has been shown experimentally for halogenated hydrocarbons in ignition studies [4], detonation studies [5], and in ignition delay calculations [6]. Wider flammability limits (typically on the lean side) in the presence of halogenated compounds have also been reported [7–10]. The pressure rise, as well as its rate, have illustrated the promotion effect of halogenated fire suppressant for some conditions [10]. Experiments with high-speed turbulent flames in a detonation/deflagration tube [11] have shown more vigorous combustion (increased deflagration/shock propagation rate or pressure ratio across the shock) for CF_3I , CF_3Br , or various hydrofluorocarbon inhibitors, with propane or ethylene fuel. Co-flow diffusion flame experiments indicated an increased total heat release with halogenated hydrocarbons added to either the fuel or the air stream [12,13]. In large-scale tests, application of water mist to a fire has been shown to cause unwanted accelerated burning [14], which was attributed to enhanced fluid-dynamic mixing. This effect has also been implicated in other tests [15]. While the possibility of enhanced flammability in the presence of hydrofluorocarbon (HFC) fire suppressants has been described, little has been done to understand the combustion enhancement. Typically, HFC agents act as fire suppressants, and based on the previous work [16,17], HFCs are expected to extinguish—or at least weaken—the FAA aerosol can test explosions. In previous work [18], thermodynamic analyses were used to predict the experimental pressure rise for addition of C_2HF_5 or $C_3H_2F_3Br$ at sub-extinguishing volume fractions (0–11.2% and 0–6%, respectively). In subsequent work [19], the kinetic behavior of CF_3Br and C_2HF_5 in the aerosol can test was studied through perfectly-stirred reactor (PSR) simulations, which were able to explain the suppression by CF_3Br , and the lack of suppression by C_2HF_5 .

The present work applies the analysis methods developed previously to understand the failure of the promising, recently introduced halon replacement agent, a perfluorinated ketone, $C_6F_{12}O$ (perfluoro(ethyl isopropyl ketone), CAS 756-13-8,

Novec 1230, FK-5-1-12, $CF_3CF_2C(=O)CF(CF_3)_2$ or $C_2F_5COC_3F_7$) in the FAA-mandated performance test. Thermodynamic calculations are used to predict the pressure rise, while perfectly-stirred reactor simulations are used to quantify the reduction in reaction rates and to understand the behavior of the chemical system with added $C_6F_{12}O$. To perform the PSR simulations, the first kinetic model for $C_6F_{12}O$ inhibition of hydrocarbon flames is developed. The work is of interest in that $C_6F_{12}O$ represents a new class of chemical (fluorinated ketones) for halon replacement (most previous agents have been fluorinated alkanes). While the present analyses are performed to understand the behavior of these fire suppressants in the FAA test, the flammability behavior of marginally flammable hydrocarbon–air–hydrofluorocarbon systems is also of interest with regard to new, marginally flammable refrigerants [20] and clean fire suppressant agents used in the presence of added energy from electrical sources [21].

2. Experiment

The FAA aerosol can test [1] simulates a fire in an aircraft cargo bay container (with a volume of 11,400 L) that heats an aerosol can (e.g., hair spray), causing it to burst and resulting in an explosion. In the FAA test, a heated container at about 16 bar, releases its contents, the typical contents of an aerosol can (ethanol, propane, and water), as a two-phase impulsive spray via a fast-acting valve. A continuous DC arc across electrodes located about 1 m downstream of the valve ignites the mixture. The fireball expands into the chamber atmosphere of premixed ambient air, water vapor, and suppressant. The temperature and pressure in the chamber increase over a time on the order of 1 s. During each test, instruments record the pressure, temperature, visual images, and concentrations of agent and oxygen. Unconfined tests without suppressants create a 3.4 m diameter fire ball [22].

3. Approach

The equilibrium conditions of the aerosol can test were calculated using CEA2 of Gordon and McBride [23]. The equilibrium simulations were used to predict the combustion temperature of the involved reactants, and the explosion pressure in the FAA test chamber, as described below (additional details can be found in Ref. [18]).

PSR simulations were used to understand kinetic limitations associated with the explosion pressure predictions of the equilibrium simulations. Flame extinction caused by suppressants is controlled by the characteristic times for chemical

reaction and transport, as described by the Damköhler number $Da = \tau_r/\tau_c$, in which τ_r is the flow residence time, and τ_c is the chemical time [24]. Hence, an important step for understanding flame suppression is to estimate the overall reaction rate. Given the explosive, two-phase, turbulent mixing process occurring during release of the aerosol can test simulator fuel [22], the reaction zone may be simulated reasonably well by a PSR. Additionally, the PSR blow-out residence time has been correlated with both the laminar flame speed [25] and with extinction of laminar diffusion flames with added inert suppressants [26], indicating its utility as a measure of overall combustion reaction rate. The residence time in the reactor is defined as $\tau_r = \rho V/\dot{m}$, in which ρ is the mixture density, V is the reactor volume, and \dot{m} is the mass flow rate. Heat losses from the reactor to the surroundings are neglected here, but could be added. The governing equations of conservation of mass, species, and energy form a system of coupled non-linear algebraic equations, which can be solved numerically. In the present work, the Sandia PSR code [27] was used. To obtain the characteristic chemical time at extinction using a stirred-reactor model, the blow-out conditions were determined, as described previously [19,26]. While any enhanced mixing in the FAA-ACT occurring due to turbulence cannot be modeled directly with the PSR simulations, the simulations can bracket the range of mixing conditions that might occur, and quantify the overall reaction rate therein.

The initial conditions for the equilibrium and stirred-reactor simulations were as follows. Initial pressure and temperature were 1.01 bar and 298 K. The calculations were performed over a range of inhibitor volume fractions, X_{inh} , in the chamber (0–10%) and fractions of chamber air, η , involved in the reaction (0.25–4.7) (experiments, but not simulations, are limited to $\eta = 1$). The relative humidity (RH) of the ambient air is known to have a significant effect on the behavior of HFCs in hydrocarbon flames owing to the sensitivity to the fluorine–hydrogen atomic ratio [20,28]. Hence, both simulations were performed for varying water vapor volume fractions (0–0.025) in the air, corresponding to 0–100% RH at 298 K. As in the FAA tests, the combustion chamber volume is 11,400 L and the FAA aerosol test can contains 5.87 mol of ethanol, 2.05 mol of propane, and 5 mol of water, all liquid.

4. Kinetic model development

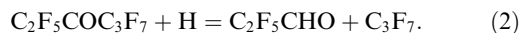
A kinetic model to examine reaction rate limitations in hydrocarbon flames inhibited by $C_6F_{12}O$ ($C_2F_5COC_3F_7$) has been developed. The kinetic model consists of four sub-mechanisms: (1) hydrocarbon combustion; (2) C_1 – C_2 fluorocarbon inhibition of hydrocarbon flames; (3) C_3 reac-

tions related to C_3F_7H (FM-200) reaction in flames; and (4) reactions related to $C_6F_{12}O$ flame decomposition, forming the fluorinated C_1 – C_3 HFC species. The hydrocarbon model adopted has been documented previously [19] and is the C_1 – C_4 model of Wang and co-workers [29], with 111 species and 784 elementary reactions. This model has been validated through comparisons with experimental ignition delay and species profiles data from shock tubes, laminar flame speeds, species profile data from flow reactors, and species profile data from flat flames. To this model, reactions related to ethanol combustion were added, based on the model of Dryer and co-workers [30] (5 species and 36 reactions). The starting mechanism to describe reactions of the hydrofluorocarbons in hydrocarbon flames is the US National Institute of Standards and Technology (NIST) HFC mechanism, including modifications suggested in more recent work, also as described in Ref. [19]. The sub-model for the flame inhibition effect of C_3F_7H was taken from Williams et al. [31] which is based on the experimental and modeling studies of Hynes et al. [32,33].

For the reactions of $C_2F_5COC_3F_7$ in flames, the decomposition pathways to the fluorinated C_1 – C_3 species present in the above sub-models were considered; these reactions and their estimated rates are listed in Table 1. Available data [32–36] show that decomposition of perfluoroacetone proceeds with formation of the perfluoroacetyl radical and perfluoroalkyl radical:



The rate constant for Eq. (1) was taken by analogy with the decomposition of perfluoroacetone [32], with adjustment of the activation energy for the enthalpy change. The displacement reaction of hydrogen atom was taken by analogy with reaction of perfluoroacetone with hydrogen atom [37]:



The rate constant for Eq. (2) was assumed to be similar to that used by Hynes et al. [32], with additional adjustment based on the data from Grattan et al. [37]. Reactions of $C_2F_5COC_3F_7$ with oxygen atom and hydroxyl radical were assumed to have rates similar to reaction with hydrogen atom. Rate constants for reaction of CH_3 and CF_3 radicals with C_2F_5CHO are from the work of Morris et al. [38].

Note that uncertainties in the decomposition chemistry of $C_2F_5COC_3F_7$ may not be critical for the conditions of flame inhibition. Because the decomposition reactions are relatively fast compared to the reactions of the decomposition products (which are responsible for the inhibition [39]), the flame inhibition and heat release effects are typically controlled by the underlying HFC

Table 1
Decomposition reactions of $C_2F_5COC_3F_7$ and its products.

Reaction	A (cm, mol, s)	E (J/mol)	Notes
$C_2F_5COC_3F_7 \rightarrow C_3F_7 + C_2F_5CO$	8.5 e16	288,700	[32] ^a
$C_2F_5CO = C_2F_5 + CO$	2.2 e13	33,500	[47,48] ^b
$C_2F_5COC_3F_7 + H = C_2F_5CHO + C_3F_7$	2.0 e12	20,900	c
$C_2F_5CHO + H = C_2F_5CO + H_2$	4.0 e13	16,700	d
$C_2F_5CHO = C_2F_5 + HCO$	4.0 e16	334,700	e
$C_2F_5COC_3F_7 + OH = C_2F_5CO + C_3F_7OH$	5.0 e12	25,100	
$C_2F_5COC_3F_7 + O = C_2F_5CO + C_3F_7O$	5.0 e12	33,500	
$CF_3 + C_2F_5CHO = CHF_3 + C_2F_5CO$	1.3 e11	28,000	[38]
$CF_3 + C_2F_5CHO = CH_4 + C_2F_5CO$	7.9 e12	41,000	[38]
$CF_3COF + CF_3 = CF_3CO + CF_4$	2.00 e12	37,700	
$CF_3COF + C_2F_5 = CF_3CO + C_2F_6$	3.00 e11	58,600	
$C_2F_6 + CF_3 = CF_4 + C_2F_5$	3.00 e12	47,300	
$CF_3CO + F = CF_3 + CF_2O$	3.00 e12	0	
$CF_3CO + F = CF_4 + CO$	5.00 e12	0	

^a Analogy with decomposition of perfluoroacetone [32]. Activation energy was adjusted for enthalpy change.

^b Analogy with decomposition of CF_3CO [47]; adjustment with the use of data in [48].

^c Similar to the displacement reaction of perfluorinated acetone [32,37].

^d Similar to the $CF_3CHO + H$ reaction.

^e Similar to CF_3CHO [32].

C_1 – C_2 species chemistry. This may not be the case for other uses of the present model, so care should be taken. Note that the overall decomposition of $C_6F_{12}O$ leads to formation of the species C_3F_7 and C_2F_5 . Thus, the inhibition effect of $C_6F_{12}O$ may represent composite effect of the suppressant agents C_2HF_5 and C_3HF_7 .

For thermodynamics, the entropies and enthalpies of formation of new species were estimated (see Table 2). Most of these data were obtained using the group additivity procedure. Enthalpies of formation of C_2F_5CHO and C_2F_5CO came from Ref. [40]. The heat of formation of $C_6F_{12}O$ was also predicted from ab initio quantum mechanical calculations (2685 kJ/mol; Smith, Personal Communication, 2011), and is close to an estimation based on group additivity (2723 kJ/mol). Because the heats of formation of dozens of HFC compounds in the NIST model are also based on group additivity, this latter value was used for $C_6F_{12}O$, providing consistency with other HFC species in the model.

The complete kinetic model for the simulations with $C_6F_{12}O$ has 1482 reactions and 180 species. For calculation of the transport properties of the

species of Table 2, the Lennard–Jones parameters were estimated using molecular weight correlations [41] and data from Ref. [42].

5. Results

5.1. Combustion temperatures

Figure 1 shows the adiabatic combustion temperature, T_{ad} , of the involved gases as a function the fraction of chamber air involved in the reaction with the fuel, with different curves corresponding to different values of X_{inh} . Note that Fig. 1 shows the combustion temperature of the involved gases; for $\eta < 1$ the final temperature of all the mixed gases would be lower due to dilution. With no agent ($X_{inh} = 0$), the shape of the curve mimics the variation in T_{ad} with fuel–air equivalence ratio, and the peak adiabatic flame temperature $T_{ad,peak}$ is reached when about one-third ($\eta = 0.29$) of the chamber volume of oxidizer reacts with the aerosol can contents. Using the data of Fig. 1, Fig. 2 shows the peak value of the $T_{ad,peak}$, as well as the value of η at which the peak occurs (η_{max}). As X_{inh} increases, $T_{ad,peak}$ increases slightly, but still remains near 2150 K, and the peak value is reached at larger values of η (due to dilution of the oxidizer by the agent, and the oxygen demand of the agent itself). For inhibitor loadings greater than $X_{inh} = 0.027$, $T_{ad,peak}$ decreases abruptly, and thereafter decreases slightly as X_{inh} increases. This occurs because $X_{inh} = 0.027 = X_{inh}|_{X/H=1}$, defined as the concentration at which $[X]/[H] = 1$, so that above this value of X_{inh} , there is not enough H atom in the system to form HF as the most stable product

Table 2
Thermochemical data for new species in $C_2F_5COC_3F_7$ decomposition sub-model.

Species	Enthalpy (kJ/mol)	Entropy (J/mol/K)	Notes
$C_2F_5COC_3F_7$	–2723	676	[49] ^a
C_2F_5CHO	–1198	391	[40] ^a
C_2F_5CO	–1033	335	[40] ^a

^a Group additivity estimation.

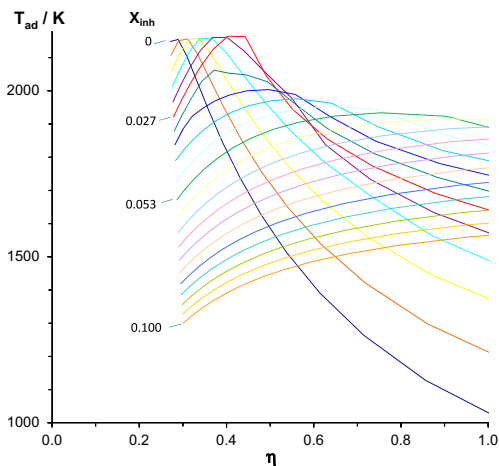


Fig. 1. Calculated adiabatic combustion temperature (T_{ad}) for fraction (η) of chamber volume involved in reaction with the aerosol can simulator fuel. Different curves refer to different initial volume fractions of the suppressant premixed in the chamber air.

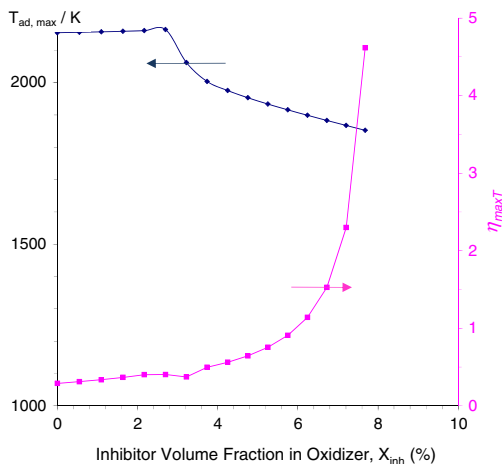


Fig. 2. Calculated maximum combustion temperature (left scale), and value of η (right scale) to achieve the peak, as a function of X_{inh} .

of fluorine, and COF_2 is typically formed, leading to less heat release. At $X_{inh} = 0.06$, $T_{ad,peak}$ is still around 1900 K, which is well within the range for typical stable hydrocarbon flames; moreover, at this agent loading, $\eta_{max} = 1$ (i.e., the entire chamber of oxidizer is required to reach peak temperature).

The fuel effect of the agent is also illustrated by considering added agent at fixed values of η . At $\eta = 0.29$, adding agent always reduces T_{ad} ; whereas for $\eta \geq 0.30$ (lean conditions with respect to the fuel in the aerosol can), adding agent first

increases T_{ad} , then lowers it at high enough X_{inh} . Thus, the agent $\text{C}_6\text{F}_{12}\text{O}$ added to the oxidizer stream acts as a fuel, with its own oxygen requirement, so that higher X_{inh} increases the volume of air-agent mixture required to consume the aerosol can test fuel. This behavior is similar to that of the agents C_2HF_5 and $\text{C}_3\text{H}_2\text{F}_3\text{Br}$, for which η_{max} also increases with X_{inh} , but in contrast to CF_3Br , for which η_{max} is constant [18].

A notable feature of this reaction system is that at high values of X_{inh} , the behavior near the peak T_{ad} is more like a plateau than a peak, such that a wide range of values of η will produce nearly the same T_{ad} . This is different from the behavior at low X_{inh} , for which T_{ad} drops off on either side of the peak, similar to the uninhibited case. Since reaction rates vary exponentially with temperature, this behavior is likely to affect the overall chemical rates at low and high X_{inh} .

Because the $[\text{H}]/[\text{F}]$ ratio in the system can affect the equilibrium products (e.g., HF vs. COF_2), and because the water vapor content of the air can vary, the equilibrium calculations were performed for a range of relative humidity in the air, from 0% RH to 100% RH (at 294 K). The effect of humidity (0% RH to 100% RH) on T_{ad} was small, less than 5% for any value of η or X_{inh} .

5.2. Explosion pressure rise

Based on equilibrium calculations, it is possible to estimate the pressure rise in the chamber [18,43]. In the calculation, a value of η is selected, and this determines the fraction of chamber volume oxidizer (air, agent, ambient water vapor) allowed to react with the fuel mix in the aerosol can simulator. An equilibrium calculation gives the conditions of the products, and these are allowed to mix adiabatically with the remaining fraction of chamber volume ($1 - \eta$), which is treated as inert.

The pressure rise at all values of η and X_{inh} was calculated; however, to estimate the expected explosion pressure rise at a given agent loading, it is necessary to estimate the actual value of η pertinent to each FAA test. In previous work [19], it was argued that the amount of involved oxidizer can be controlled by either the turbulent mixing resulting from the impulsive release of the aerosol can simulator contents, or by diffusion (as in a laminar diffusion flame). It was shown that for the agents C_2HF_5 and $\text{C}_3\text{H}_2\text{F}_3\text{Br}$, assuming diffusion flame behavior (such that the ratio of oxidizer to fuel was that which gave the peak temperature) predicted the pressure rise very well. Hence, that assumption is adopted in the analyses below for $\text{C}_6\text{F}_{12}\text{O}$.

Figure 3 shows the predicted pressure rise for $\text{C}_6\text{F}_{12}\text{O}$ in the FAA-ACT (FAA experimental results: solid circles; predicted value: lines). The agreement is reasonable considering the

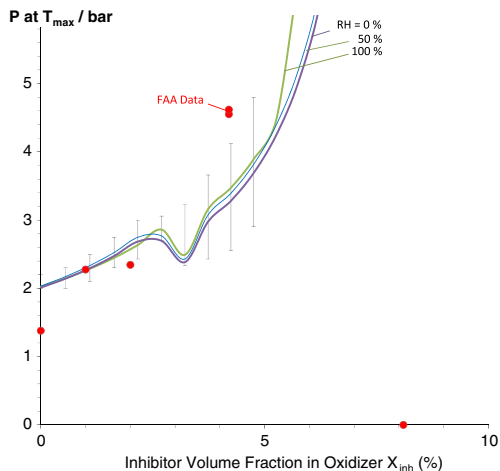


Fig. 3. Calculated explosion pressure (lines) and FAA measurements (dots).

simplifications in the model; however, the experimental pressure rise at $X_{inh} = 0.042$ is somewhat underpredicted. While water vapor can have some effect (as shown by the difference in the lines for 0% and 100% RH), errors in the predicted η_{max} have a much larger effect. For example, the error bars in the curve for $C_6F_{12}O$ show the variation in the pressure rise due to uncertainties in η , which are estimated as follows. Figure 1 shows that for values of $X_{inh} > X_{inh}|_{X/H=1}$, the temperature near the peak is very flat; that is, a wide range of values of η give nearly the same value of the peak temperature. For example, with 4.2% $C_6F_{12}O$, values of η from 0.42 to 0.72 produce combustion temperatures within 2% (40 K) of the peak value. As shown in Fig. 3, these differences in η can imply explosion pressures ranging from 2.6 to 4.1 bar (39 to 61 psig) for $C_6F_{12}O$. Hence, it is possible that uncertainties in the estimate of the actual value of η that occurs in the FAA test are responsible for the discrepancy between the predicted and actual explosion pressure.

The equilibrium calculations used to estimate the pressure rise shown in Fig. 3 are based on the assumption of complete reaction to equilibrium products. Apparently, kinetic limitations do not influence the system until a $C_6F_{12}O$ volume fraction of 8.1%, at which there is no pressure rise. As shown in Fig. 2, at $X_{inh} = 0.077$, $\eta_{max} = 4.6$, so that at $X_{inh} = 0.081$, the system is very fuel rich (with an overall equivalence ratio above 5); i.e., the system is likely beyond the rich flammability limit. As Fig. 3 implies, below $X_{inh} = 0.042$, kinetic limitations to the reaction of the agent are unlikely. This is somewhat surprising, since cup burner flames of *n*-heptane are extinguished at $X_{inh} = 0.045$ [44]. To understand the effects of $C_6F_{12}O$ on the overall reaction rate of the FAA

aerosol can test chemical system, PSR simulations were performed, as described below.

5.3. Perfectly-stirred reactor calculations

Figure 4 shows the characteristic overall reaction rate at blowout in the PSR, ω_{psr} (which is equal to the inverse of the residence time in the reactor just above the blowout condition [19]), as a function of η for the FAA-ACT (different curves refer to different values of X_{inh}). With no inhibitor ($X_i = 0$ curve), ω_{psr} is very sensitive to η (i.e., the stoichiometry); whereas for higher X_{inh} , ω_{psr} is less sensitive to η (the curves flatten out at higher X_{inh}). Conversely, the effect of X_{inh} on ω_{psr} is dependent upon the value of η : for $\eta < 0.5$, (richer conditions), adding inhibitor always lowers ω_{psr} ; whereas for $\eta \geq 0.5$, (fuel lean), increasing X_{inh} first raises the ω_{psr} , and then at high X_{inh} , lowers ω_{psr} . In other words, at high η adding inhibitor can increase the overall reaction rate in the system, rather than decrease it as would be expected for a fire suppressant. Apparently, the influence of increasing temperature with added agent (shown in Fig. 1) overrides inhibition effect due to H-atom scavenging by fluorinated species. Moreover, for $0.052 \leq X_{inh} \leq 0.10$, the curves are very close, so that added inhibitor above $X_{inh} = 0.052$ has a smaller effect on the overall reactivity (i.e., the marginal effectiveness of $C_6F_{12}O$ appears to be diminished at higher X_{inh}). Hence, at low inhibitor loadings and over-ventilated conditions, adding agent makes the system more reactive, and at higher loadings, higher concentrations have little effect on the reactivity. Both effects can explain the lack of effective inhibition with added $C_6F_{12}O$ in the FAA-ACT. PSR simulations at different volume fractions of ambient water vapor indicate that an increase in humidity from 0% to 50% can enhance the reactivity of the system,

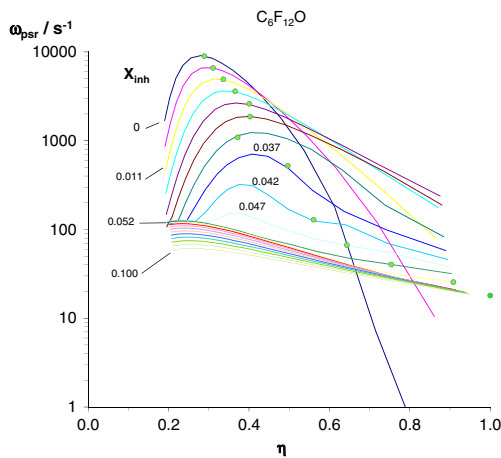


Fig. 4. Overall chemical rate ω_{psr} vs. η .

especially at higher η and X_{inh} near but slightly greater than $X_{i|X/H=1}$, where ω_{psr} is increased by 15–30%. Hence, the large amounts of water in the FAA-ACT may be enhancing the reactivity of the system at high agent loadings.

As discussed above, the value of η relevant to the FAA-ACT experiments can be estimated from the experimental explosion pressure rise observed, using the equilibrium calculations that predicted the FAA pressure rise. The value of η_{max} required to produce the $T_{ad,max}$ for a given value of X_{inh} is shown by the green dots in Fig. 4. As illustrated, the value of η_{max} increases with X_{inh} , and the overall chemical rate decreases (although at a slower rate at higher X_{inh}).

Examining the value of X_{inh} for which the explosion was suppressed ($X_i = 0.081$) is instructive. For this condition, the entire chamber volume is required for peak T_{ad} (which, as Fig. 2 shows, is true for $X_{inh} > 0.06$). Hence, the system was overall air starved, which may have been the cause of suppression rather than kinetic limitations due to fluorine species reactions [39]. From Fig. 4, at the inerting concentration for $C_6F_{12}O$ ($X_{inh} = 0.081$), $\eta = 1$ and $\omega_{psr} = 16 \text{ s}^{-1}$; for comparison, at the inerting concentration for C_2HF_5 ($X_i = 0.135$), η is again 1.0, and $\omega_{psr} = 0.22 \text{ s}^{-1}$ [19]. These values are remarkably close, considering that the inerting concentration was not resolved very well in either case, and the analysis has many simplifications. Interestingly, we can also compare ω_{psr} (51 and 75 s^{-1}) for C_2HF_5 and $C_6F_{12}O$ at the minimum extinction concentration for cup-burner flames with these agents ($X_i = 0.113$ and 0.053 [3], respectively); again, the values in the PSR simulation scale very well with those of the experiment. The present findings for $C_6F_{12}O$ are consistent with, and support the findings of earlier analyses for the behavior of C_2HF_5 and CF_3Br in the FAA-ACT. The characteristic chemical rate ω_{psr} obtained from stirred-reactor simulations is a good metric for quantifying the characteristic reaction rate relevant to flame extinguishment for both the FAA-ACT and the cup burner, for the chemical systems involved. Consequently, detailed analysis of the chemical reaction pathways in the PSR simulations should allow further insights into this surprising behavior.

6. Conclusions

The unusual combustion enhancement observed in the FAA aerosol can test experiments with the fire suppressant $C_6F_{12}O$ has been studied. A kinetic model for the behavior of $C_6F_{12}O$ in hydrocarbon flames has been developed, and the mechanisms of combustion enhancement have been suggested.

Perfectly-stirred reactor simulations, over a wide range of inhibitor concentration and fuel-oxidizer ratio, have shown that adding the suppressant to a lean system not only adds energy to the system (and enhances the heat release, as would be expected [45]), but increases the overall reaction rate as well. Given the very high agent loading for these conditions, and despite the resulting low overall reactivity calculated with the PSR simulations, the existence of sustained combustion in the FAA test is telling. Apparently, the heat losses and residence time in this particular configuration are such that even chemical systems with low reactivity (i.e., with very low burning velocity) must be considered. Also, it is likely that the turbulent, non-premixed flame structure of the FAA test influences the combustion which can occur (and is being addressed in parallel work [46]).

Acknowledgements

Helpful conversations with John Reinhardt at the FAA Technical Center, and Jeff Manion, Wing Tsang, and Don Burgess, John Pagliaro at NIST are gratefully acknowledged. The work was supported by the Boeing Company.

References

- [1] J.W. Reinhardt, *Behavior of Bromotrifluoropropene and Pentafluoroethane When Subjected to a Simulated Aerosol Can Explosion*, DOT/FAA/AR-TN04/4, Federal Aviation Administration, 2004.
- [2] J.W. Reinhardt, *Minimum Performance Standard for Aircraft Cargo Compartment Halon Replacement Fire Suppression Systems (2nd Update)*, DOT/FAA/AR-TN05/20, Federal Aviation Administration, 2005.
- [3] J.W. Reinhardt, Aircraft Cargo MPS Test of FK-5-1-12, International Aircraft Systems Fire Protection Working Group, Federal Aviation Administration, October 25–26, 2006.
- [4] L.A. Lovachev, V.T. Gontkovskaya, N.I. Ozerkovskaya, *Combust. Sci. Technol.* 17 (1977) 143–151.
- [5] I.O. Moen, P.A. Thibault, J.H. Lee, R. Knystautas, T. Dean, C.K. Westbrook, *Proc. Combust. Inst.* 20 (2008) 1717–1725.
- [6] V.I. Babushok, D.R.F. Burgess, W. Tsang, A.W. Miziolek, in: W. Tsang, A.W. Miziolek (Eds.), *Halon Replacements*, ACS Symposium Series, vol. 611, American Chemical Society, Washington, DC, 1995.
- [7] N. Saito, Y. Saso, C.H. Liao, Y. Ogawa, Y. Inoue, in: W. Tsang, A.W. Miziolek (Eds.), *Halon Replacements*, ACS Symposium Series, vol. 611, American Chemical Society, Washington, DC, 1995.
- [8] T.A. Moore, D.S. Diedorf, S.R. Skaggs, in: *Proceedings of the 1993 CFC & Halon Alternatives Conference*, 1993.

- [9] S. Kondo, K. Takizawa, A. Takahashi, K. Tokuhashi, A. Sekiya, *Fire Saf. J.* 44 (2009) 192–197.
- [10] Y.N. Shebeko, V.V. Azatyan, I.A. Bolodian, et al., *Combust. Flame* 121 (2000) 542–547.
- [11] G. Gmurczyk, W. Grosshandler, *Proc. Combust. Inst.* 25 (1994) 1497–1503.
- [12] G. Holmstedt, P. Andersson, J. Andersson *Fire Safety Science—Proceedings of the Fourth International Symposium*, vol. 4, International Association of Fire Safety Science, 1994, pp. 853–864.
- [13] V.R. Katta, F. Takahashi, G.T. Linteris, *Combust. Flame* 144 (2006) 645–661.
- [14] J.R. Mawhinney, B.Z. Dlugogorski, A.K. Kim *Fire Safety Science—Proceedings of the Fourth International Symposium*, vol. 4, International Association of Fire Safety Science, 1994, pp. 47–60.
- [15] A. Hamins, K. McGrattan, G.P. Forney, *Unwanted Accelerated Burning After Suppressant Delivery*, SP-1004, National Institute of Standards and Technology, 2003.
- [16] D. Treese, K. Seshadri, A. Hamins, in: A.W. Miziolek, W. Tsang (Eds.), *Halon Replacements: Technology and Science*, ACS Symposium Series, vol. 611, American Chemical Society, Washington, DC, 1995.
- [17] E.J.P. Zegers, B.A. Williams, E.M. Fisher, J.W. Fleming, R.S. Sheinson, *Combust. Flame* 121 (2000) 471–487.
- [18] G.T. Linteris, F. Takahashi, V.R. Katta, H.K. Chelliah, O. Meier, *Int. Assoc. Fire Saf. Sci.* (2011) 1–14.
- [19] G.T. Linteris, D.R. Burgess, V.R. Katta, F. Takahashi, H.K. Chelliah, O. Meier, *Combust. Flame* 159 (2012) 1016–1025.
- [20] K. Takizawa, A. Takahashi, K. Tokuhashi, S. Kondo, A. Sekiya, *Combust. Flame* 141 (2005) 298–307.
- [21] G.T. Linteris, *Fire Technol.* 47 (2011) 1–68.
- [22] T. Marker, *Initial Development of an Exploding Aerosol Can Simulator*, DOT/FAA/AR-TN97/103, Federal Aviation Administration, 1998.
- [23] S. Gordon, B.J. McBride, *Computer Program for Calculation of Complex Chemical Equilibrium Compositions and Applications*, NASA Reference Publication 1311, NASA Glenn Research Center, 1996.
- [24] F.A. Williams, *J. Fire Flammability* 5 (1974) 54–63.
- [25] R.B. Barat, *Chem. Eng. Sci.* 56 (2001) 2761–2766.
- [26] S. Liu, M.C. Soteriou, M.B. Colket, J.A. Senecal, *Fire Saf. J.* 43 (2008) 589–597.
- [27] P. Glarborg, R.J. Kee, J.F. Grcar, J.A. Miller, *PSR: A FORTRAN Program for Modeling Well-Stirred Reactors*, SAND86-8209, Sandia National Laboratories, 1986.
- [28] G.T. Linteris, in: A. Miziolek, W. Tsang (Eds.), *Halon Replacements*, ACS Symposium Series, vol. 611, American Chemical Society, Washington, DC, 1995.
- [29] H. Wang, X. You, K.W. Jucks, et al., USC Mech Version II. High-Temperature Combustion Reaction Model of H₂/CO/C₁–C₄ Compounds, University of Southern California, 2007, available at http://ignis.usc.edu/USC_Mech_II.htm.
- [30] J. Li, A. Kazakov, F.L. Dryer, *J. Phys. Chem. A* 108 (2004) 7671–7680.
- [31] B.A. Williams, D.M. L'esperance, J.W. Fleming, *Combust. Flame* 120 (2000) 160–172.
- [32] R.G. Hynes, J.C. Mackie, A.R. Masri, *Combust. Flame* 113 (1998) 554–565.
- [33] R.G. Hynes, J.C. Mackie, A.R. Masri, *J. Phys. Chem. A* 103 (1999) 54–61.
- [34] R.M. Robertson, D.M. Golden, M.J. Rossi, *J. Phys. Chem.* 92 (1988) 5338–5347.
- [35] N. Taniguchi, T.J. Wallington, M.D. Hurley, A.G. Guschin, L.T. Molina, M.J. Molina, *J. Phys. Chem. A* 107 (2003) 2674–2679.
- [36] E. Abuin, E.A. Lissi, *J. Photochem.* 5 (1976) 65–68.
- [37] D.W. Grattan, K.O. Kutschke, *Can. J. Chem.* 56 (1978) 2638–2645.
- [38] E.R. Morris, J.C.J. Thynne, *Trans. Faraday Soc.* 64 (1968) 3027–3034.
- [39] G.T. Linteris, D.R. Burgess, V. Babushok, M. Zachariah, W. Tsang, P. Westmoreland, *Combust. Flame* 113 (1998) 164–180.
- [40] Y. Wang, J.Y. Liu, L. Yang, X.L. Zhao, Y.M. Ji, Z.S. Li, *J. Mol. Struct. THEOCHEM* 820 (2007) 26–34.
- [41] H. Wang, M. Frenklach, *Combust. Flame* 96 (1994) 163–170.
- [42] O. Setokuchi, S. Kutsuna, M. Sato, *Chem. Phys. Lett.* 429 (2006) 360–364.
- [43] R.A. Ogle, *Process Saf. Prog.* 18 (1999) 170–177.
- [44] B.P. Carnazza, J.G. Owens, P.E. Rivers, J.S. Schmeer, in: National Institute of Standards and Technology, 2004.
- [45] E.A. Ural, *Process Saf. Prog.* 22 (2003) 65–73.
- [46] F. Takahashi, G.T. Linteris, V.R. Katta, O. Meier, *Proc. Combust. Inst.* 34 (2012).
- [47] R.G. Hynes, J.C. Mackie, A.R. Masri, *Energy Fuels* 13 (1999) 485–492.
- [48] R.L. Waterland, K.D. Dobbs, *J. Phys. Chem. A* 111 (2007) 2555–2562.
- [49] S.E. Stein, J.M. Rukkens, R.L. Brown, NIST Standard Reference Database 25: NIST Structures and Properties Database and Estimation Program, National Institute of Standards and Technology, 1991.